Convective mitigation of dendrite growth

Oles Dubrovski
Interdisciplinary Graduate Program in Applied Mathematics, Technion, Haifa 32000, Israel

Ofer Manor*
Department of Chemical Engineering, Technion, Haifa 32000, Israel

(Received 15 August 2021; accepted 10 December 2021; published 30 December 2021)

The growth of metallic dendrites during the electrodeposition and solidification of metal films is a formidable scientific and industrial problem. It is mostly known for hindering the use of high energy-density solid metal electrodes in rechargeable batteries. Over a century ago, it was experimentally shown that metallic dendrites may be mitigated under the action of mass advection in the liquid adjacent to a solid metal surface which grows out of a melt. Similar observations were reported for electrochemical deposition four decades ago and very recently. However, these insights proved inconclusive; dendrites appear to grow to different extents in many advection-based deposition systems, such as flow batteries, augmented finger batteries, and convective solidification. Here, we scrutinize the contribution of high Peclet metal ion convection in a dilute solution to the growth rate of metal dendrites, emphasizing convective effects near the metal surface. We employ an ideal model system for the isothermal flow of an ion solution along a duct where ions desorb from one solid surface of the duct, transport through the solution, and adsorb (undergo deposition) onto the other side. To account for the limit where metal-ion transport through the solution is the bottleneck for the rate of metal deposition (contributions to dendrite mitigation from near equilibrium surface phenomena are assumed small), we employ the perspective of *kinetic stability* to elucidate the contribution of ion convection to the mitigation of dendrite growth. We show that while the convection of metal ions appears to enhance dendrite growth — an intuitive insight — it also enhances the growth of the bulk solid metal on which the dendrites grow — a well-known phenomenon. We demonstrate that for a fixed growth rate of the bulk solid metal, the rate of growth of dendrites is smaller in the presence of convective flow compared to the case where ion transport is solely by diffusion. The difference in the relative rate of growth in the presence and absence of convective flow may span orders of magnitude, which explains the absence of significant dendrites in corresponding experiments.

DOI: 10.1103/PhysRevMaterials.5.123402

I. INTRODUCTION

Inhibiting the growth of micron to millimeter size tree-like morphological structures, dendrites, is an old scientific problem which still hinders many technological advancements [1,2]. The growth of dendrites during the electrodeposition of metal mass on electrodes for charging batteries or coating surfaces inhibits the use of high-energy density metal electrodes in finger batteries [3], constrains the design and efficiency of flow batteries [4], and inhibits exquisite control over surface morphology in metallic coatings [5]. In particular, Li metal is touted to be one of the most promising materials for the next-generation rechargeable batteries [6]. Yet applications are still not a practical technology due to the formation of dendrites during the recharge process. Moreover, the growth of dendrites during the precipitation of metal alloy mass influences the microstructure and thereby the mechanical and chemical behaviors of materials [7], and degrades energy storage capacity as latent heat [8,9].

Dendrites grow from interfacial irregularities like geometrically or chemically nonuniform solid surface as in the case of a fractured solid-electrolyte interfacial (SEI) passivation layer [10]. The growth of a dendrite may be divided into three steps [11]. These are the nucleation of dendrites in the metal, the protrusion or deformation of the metal surface by the nucleus which serves as a hotspot for the third step: macroscopic growth. Moreover, the lack of lithium salt to create SEI on the deposited lithium causes the growth of initial surface protrusions into dendrites, or a transition between a mossy growth into dendritic growth [12–14]. In addition, the generation of gas during the deposition of ions may further affect the surface morphology [15,16]. It is difficult to control surface growth in the first and third steps. Hence, we explore the initial dendrite growth from a hotspot at the metal surface.

The growth of dendrites is driven by the transport of ions and their adsorption to a solid surface. Their adsorption may be resisted by near equilibrium surface phenomena, such as the excess free energy at the metal surface and its curvature, alongside pressure in the electrolyte solution and mechanical stress in the solid [11,17,18]. Hence, the growth of dendrites may be divided into two limits: one is reaction-limited and the other is transport-limited. In the reaction-limited case, the bottleneck for the rate of metal growth is the rate of adsorption of metal ions to the metal surface. Dendrite-resisting mechanisms, like the ones we mention above, play an important role

*Corresponding author: manoro@technion.ac.il

in shaping the morphology of the metal surface. An example for irregular growth of a lithium-metal electrode during electrodeposition in this case is the growth of a mossy structure on the electrode, which is caused by the release of stress beneath the SEI. In the transport-limited case, the bottleneck for the growth of the metal surface is the rate of metal-ion transport through the electrolyte solution. This case is associated with small contributions from dendrite resisting mechanisms in or at the surface of the solid metal. An example for this case is the limiting current condition in electrodeposition, which is known to be susceptible to fast dendrite growth.

Many studies on the stability of dendrite growth assume the diffusive and migrative transport of ion mass to a growing bulk solid metal. Examples are studies [11,19,20] on electrodeposition in liquid and solid electrolytes. Surface conduction is another mechanism that has the potential to eliminate dendrites [21]. However, the mass transport of metal ions to a solid surface during both electrodeposition and solidification from a solution (precipitation) may further undergo convective transport, such as forced convection, electroconvection, and natural convection [22–24], where each mechanism may contribute differently to morphological stability. The most well-known corresponding systems are solidification [25], flow batteries [26], and water desalination [27]. A flow field in a liquid electrolyte may introduce a significant contribution to the morphology of the solid metal and may corrugate or smooth the metal surface [28,29].

In 1916, Czochralski *et al.* showed that to avoid dendrite growth, it is advantageous to introduce stirring to the melt during the procedure of silicon crystalization [25,30–32]. However, Tajima and Ogata [33] observed dendrites growing in the direction of electrolye flow during the electrodeposition of inert metals in aqueous solutions under various concentrations of electrolyte, electrical current densities, and temperatures. Following up on this work, Jorne *et al.* [18] investigated the influence of flow on the morphology of zinc electrodeposition atop a (flow-through) porous electrode. The impinging flow appeared to significantly suppress dendrites. A faster electrolyte flow velocity yielded a smaller surface roughness. The stabilizing effect of the impinging flow shown in the previous work was verified theoretically by Parekh [34]. Moreover, a recent work by Huang *et al.* [3], which explored the actuation of microflows by acoustic excitation in Li metal finger batteries, reported the elimination of dendrites during battery recharge. Additional studies considered the influence of Couette- and Poiseuille-type flows on morphological stability [35,36], showing that this type of cross flow reduces metal dendrite growth considerably, but does not entirely prevent it [35].

Studies on an isolated, single, growing dendrite during the solidification of solid melt, appear to observe that flow in the liquid enhances its rate of growth [37]. Ananth and Gill [38,39] used theory to observe that thermal convection is significant in the case of a weak supercooling conditions, where they suggested that the growth rate of the dendrites is determined solely by the temperature gradient at its tip. In addition, studies on the stability of the shape of a single growing dendrite under convective flow were performed by Bouissou *et al.* [40] for small "growth Peclet numbers" and expanded by Alexandrov *et al.* [41,42] to an arbitrary "growth Peclet numbers," binary mixtures, and antisotropic surface energy. Considering both contributions from surface phenomena and convective flow, they also observed that the convective flow increases the rate of growth of the single dendrite.

Studies on the morphological stability of planar surfaces during solidification and under the influence of crossflow suggest otherwise: Delves [43] assumed a parabolic velocity profile in the thermal boundary layer near the solid-liquid interface and showed that flow in the liquid melt will suppress morphological instabilities. However, Coriel *et al.* [44] suggested that strong mixing flow in the liquid melt may enhance nonplanar growth in the likely case in which the concentration of metal ions in the carrier liquid is smaller than the concentration of metal atoms in the solid. They assumed an effective flow-stagnant diffusion layer whose predefined constant thickness near the solid-liquid interface is determined by the shear rate of flow in the liquid.

Here, we solve a problem of dendrite growth at a surface of a duct that undergoes a convective Poiseuille-type flow in a solution of ions. The ions transport from one side of the duct to the other. We employ this model system in an attempt to resolve the distinct contradiction between different studies as to the contribution of convective flow in a solution to the rate of dendrite growth in the cases of solidification from a solution and electrodeposition. We concentrate on the question whether the convection of metal ions in a solution supports or mitigates the growth of dendrites when compared to the transport of ions in the solution by pure diffusion. In particular, we assume an ideal model system to predominantly concentrate on the direct contributions of ion convection to the rate of dendrite growth. Hence, to avoid masking the dendrite growth by the many additional mechanisms that take place in industry-level electrodeposition and solidification systems, we assume a dilute and isothermal solution of ions, small geometrical protrusions that serve as hotspots for dendrite growth, and avoid dendrite-stabilizing mechanisms at the solid surface and within the solid metal by considering the regime where the transport of ions through solution towards a solid metal surface is the rate-determining mechanism for the rate of growth of the solid. The above simplifying assumptions will prove inadequate for most realistic systems in use but allow us to concentrate on the pure distribution of convective flow in a solution of ions to the rate of growth of dendrites with relevance to both electrodeposition and solidification from a solution of ions. Hence, in Secs. II and III, we suggest and solve the model equations to our problem. In Sec. IV, we employ the concept of *kinetic stability* to quantify the contribution of the initial dendrite hotspot density and flow velocity in the solution to the rate of growth of dendrites and of the bulk solid metal. In Sec. V, we give a summary of our work and insights.

II. MODELING

A. Problem description

We solve a problem of metal dendrite growth at a bottom surface of a duct that undergoes a convective Poiseuille-type flow while ions transport in a dilute solution from the upper surface of the duct to its lower surface. Using this ideal model

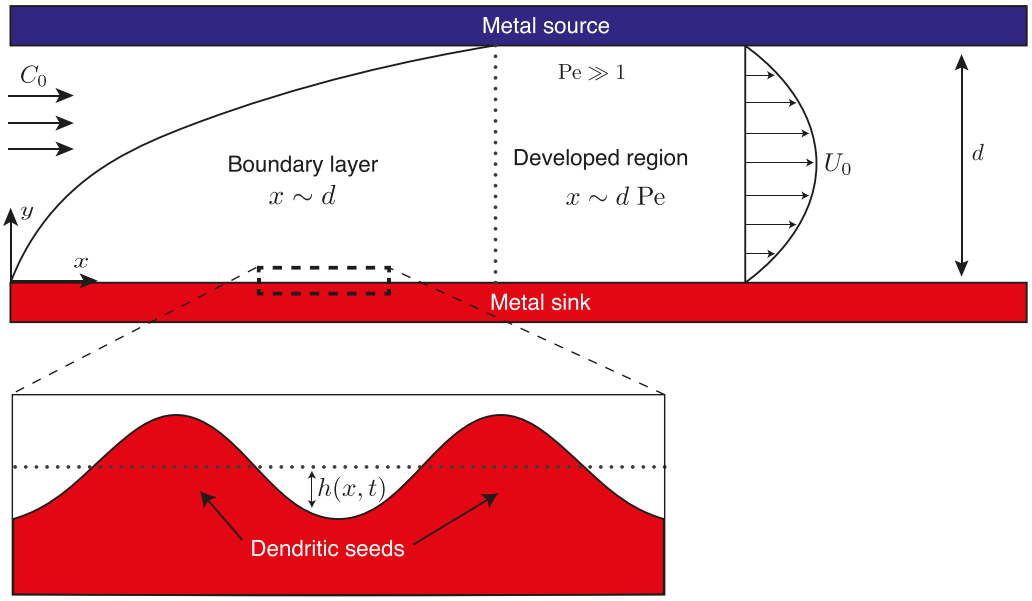

FIG. 1. Large Peclet (Pe) number convection of metal ions, which enter a 2D, rectangular, duct of an inner thickness d at a concentration $C = C_{\text{in}}$ by a Poiseuille-type flow of a center-line velocity U_0, where The lower and upper sides of the duct serve as a sink and a source of metal ions (a cathode and an anode in the case of electrodeposition), respectively, and where the lower side supports geometrical hotspots for dendrite growth, which we illustrate in the inset by the sinusoidal protrusions (roughness) $h(x,t)$ of wavelength k. We assume that the ion solution is dilute and isothermal, the dendrite protrusions are small, and that the rate by which ions adsrob to the bottom metal surface which serves as ion sink is limited by the rate of ion transport through the solution. Upstream we illustrate a concentration boundary layer and downstream we illustrate a concentration-developed region past the boundary layer.

system, we explore the contribution of forced mass convection to dendrite growth in the regime where the rate of metal ion attachment to the solid metal surface is determined solely by the rate of ion flux, i.e., the rate of ion attachment to the solid surface is transport-limited. Hence, we assume that the contribution of near equilibrium surface phenomena to the adsorption of ions to the solid surface, such as surface tension and surface curvatures, is small. Our model system may be associated with limiting cases of electrodeposition and solidification from a solution (precipitation).

In the case of electrodeposition, reaction kinetics at the electrodes are many times assumed to be governed by the extended Butler-Volmer equation [20]. Sufficiently high cell voltage difference between the electrodes reduces the extended Butler-Volmer equation to a statement in which the rate of ion adsorption to the metal electrode is governed by ion transport through the electrolyte solution. Assuming that the voltage difference is not too large to invoke a significant space-charge layer (whose contribution may be further alleviated using the presence of supporting electrolytes) or electroconvection [45,46], we may specify the concentration at the electrode to be $C \approx 0$, to leading order. This condition is known as the *limiting current* condition. We assume an isothermal solution of constant density and a simple surface reaction of the adsorbing metal ions with no side products, so that we avoid possible gas evolution effects. We further assume small protrusions (hotspots for dendrite growth) at the solid surface, which render their radius of curvature large and electroconvection effects small.

Solidification systems exhibit dendrite formation in a similar manner to electrodeposition, albeit in the absence of an electric field. Similar assumptions may be taken to investigate simple solidification from a solution. In particular, the assertion of an isothermal solution is compatible with the assumption of small protrusions in the solid surface in this case. The Gibbs-Thomson effect, $T = T_0 - (T_0/Q) \times (\sigma/R)$, gives the melting temperature of a curved solid surface, in which σ, Q, and $1/R$ are the liquid-solid surface tension, latent heat, and surface curvature of the solid, respectively, and T_0 is the flat interface melting temperature. That is, sufficiently small protrusions in the solid surface, which satisfy large radius of curvature, $1/R \ll 1$, render σ/QR small and the nearly flat solid surface isothermal to leading order.

The geometry for our model is depicted in Fig. 1. Metal ions transport in a liquid phase through a Poiseuille-type flow in a two-dimensional duct. The duct is initially of an inner thickness d. Ions are advected by the flow of solution from left to right, and are released from the upper side of the duct and adsorb onto the lower side of the duct. In the case of electrodeposition, the lower and upper sides are a cathode and an anode, respectively. For simplicity we assume that the metal concentration in the solution at the entrance to the duct $C = C_{\text{in}}$ is the same as the one at the upper side of the duct. Moreover, noted above, we ignore thermal effects which may be considerably more important in the case of solidification, however, we will devoid this work from the simple and generic insights we seek.

We assume that the transport of mass by advection is considerably more prominent than by diffusion, that is, a large Peclet number, which is, for example, a characteristic of flow batteries. Metal ions are consumed at the surface of the metal sink, hence, we expect a concentration boundary layer upstream and near the lower side of the duct. To leading order, the concentration of mass between the boundary layer and the

upper side of the duct is approximately the inlet concentration $C = C_{\rm in}$. The concentration of metal ions at the boundary layer is reduced when approaching the bottom of the duct. The thickness of the boundary layer increases downstream until it reaches the upper side of the duct. Further downstream, past the concentration boundary layer, the qualitative behavior of the flux of mass to the lower side of the duct changes considerably. To account for dendrite hotspots, we assume the presence of minor harmonic deformities (protrusions) at the solid surface, which alter the concentration field in the duct and hence their own rate of growth. In what follows, we first discuss the case of a concentration boundary layer near the upstream edge of the metal surface (at the entrance to the duct) and then we discuss the region past the boundary layer.

B. Concentration boundary layer

Here we consider the concentration boundary layer near the upstream edge of the metal surface at the entrance to the duct. Rendering the problem dimensionless, we employ the transformations for the concentration field $C \to C_{\rm in}C$ the Cartesian coordinates and the position of the metal surface $(\mathbf{x}, h) \to d(\mathbf{x}, h)$, the velocity field $\mathbf{u} \to U\mathbf{u}$, and time, $t \to (d^2/DC_{\rm in}v_s){\rm Pe}^{-2/3}t$, where U is the characteristic flow velocity, v_s is the molar volume of the solid metal, D is the diffusion coefficient of the metal ions, ${\rm Pe} \equiv UC_{\rm in}/D \gg 1$ is the Peclet number, and the timescale is associated with the rate of growth of the solid metal surface. Both $\mathbf{x} \equiv (x, y)$ and $\mathbf{u} \equiv (u, v)$ are comprised of two components which are along and transverse the duct, respectively. In particular, the scale of time is chosen so that we concentrate on the rate of growth of the solid metal at the bottom of the duct. The distribution of metal ion concentration is governed by the transport equation

$$C_{\rm in}v_s\,{\rm Pe}^{-1/3}\,\partial C/\partial t + \mathbf{u}\cdot\nabla C = \frac{1}{\rm Pe}\nabla^2 C, \qquad (1)$$

where the absence of electrophoresis in the case of electrodeposition is compatible with the presence of supporting electrolytes, which are usually introduced to reduce ohamic resistance. The dimensionless number $C_{\rm in}v_s \ll 1$ is the ratio between the concentration of metal in the liquid solution and in the solid, and is assumed to be a small number. Hence, dynamic contributions to the transport of metal in the solution may be neglected in our analysis. The dimensionless metal concentration at the entrance to the duct and near its upper side is $C(x, y = d) = C(x = 0, y) = 1$ and near its lower part is $C(x, y = h) = 0$.

The rate of metal growth is determined by the flux of metal ions near the bottom solid surface

$$\partial h/\partial t = -\nabla C\cdot\boldsymbol{n}|_{y=h} - C_{\rm in}v_s{\rm Pe}^{2/3}C|_{y=h}\boldsymbol{u}^I\cdot\boldsymbol{n}, \qquad (2)$$

where $\boldsymbol{u}^I\cdot\boldsymbol{n} \approx \partial h/\partial t$ is the velocity of flow near the solid surface to result from its rate of growth and $\mathbf{n}$ is the outer normal to the metal surface. The limit of a dilute solution of metal ions, where $C_{\rm in}v_s \ll {\rm Pe}^{-2/3}$, renders the right-most convective term in the equation small.

We model the dendrite seeds as harmonic undulations $h_1(x, t)$ about the baseline of the metal surface at the bottom of the duct, $h_0(x, t)$. We assume that the thickness of the metal solid at the lower part of the duct takes, at short times, the form

$$\begin{aligned} h(x, t) &= {\rm Pe}^{-1/3}h_0(x, t) + \epsilon h_1(x, t) + \cdots \\ &\approx {\rm Pe}^{-1/3}h_0(t) + \epsilon f(t)\sin(kd\,x) + \cdots . \end{aligned} \qquad (3)$$

The magnitude of the leading-order component in the series, given by ${\rm Pe}^{-1/3}$, is a consequence of the concentration boundary layer, to be elaborated in the followings. In addition, $\epsilon = l/d$ is a small parameter which gives the initial ratio between the height of the dendrite seeds, l, relatively to the duct thickness, d, and k is a wave number which corresponds to the surface density of hotspotes for dendrite growth. We further assume that at short times the geometry of the dendrite hotspots may be considered harmonic and that the baseline of the bulk solid metal is predominantly a function of time and hence nearly flat, which simplifies the analysis of the velocity field.

The flow in the duct is assumed to be an incompressible Poiseuille-type flow of a constant density liquid. The characteristic Reynolds number of convective flow in finger batteries and in flow batteries is approximately of unity order of magnitude. For simplicity we employ in our analysis Stokes flow to model the perturbation of the flow by the dendrite hotspots. The corresponding equation that governs the flow in this case is $\nabla^4\psi = 0$, where the stream-function ψ satisfies the flow velocity along and transverse to the surface of the duct $\mathbf{u} \equiv (u, v) = (\psi_y, -\psi_x)$, respectively. The streamline equation is rendered dimensionless by employing the transformation $\psi \to Ud\Psi$. The conditions of no-slip flow and no penetration of liquid at the solid boundaries $\mathbf{u}\cdot\mathbf{n}|_{y=h(x),d} = 0$ and $\mathbf{u}\cdot\mathbf{t}|_{y=h(x),d} = 0$, respectively, yield the velocity field [47]

$$\begin{aligned} \psi = \frac{y^2}{4} - \frac{y^3}{6} - \frac{\epsilon\sin(kdx)}{2(-2kd^2 + \cosh(2kd) - 1)} \\ \times \{2kd(y-1)\sinh(kdy) + y\cosh[kd(y-2)] \\ - y\cosh(kdy)\}, \end{aligned} \qquad (4)$$

where $\mathbf{t}$ is the tangent unit vector to the surfaces of the duct. In particular, inline with Eq. (2), we ignore contributions to the flow field from the moving metal surface $\partial h/\partial t$ subject to our assumption of a dilute ion concentration in the solution, i.e., $C_{\rm in}v_s \ll 1$.

The leading-order problem $\mathcal{O}(1)$, which is comprised from Eqs. (1) to (4), where we omit any term which is multiplied by the small parameters ϵ and $C_{\rm in}v_s$, is a classic Leveque problem [48,49] and is devoid of the presence of dendrites. The upper part of the duct — the outer region — is dominated by advective ion transport. The bottom part — the inner region — is a concentration boundary layer. In the boundary layer, the relevant lengthscale transverse to the duct $Y = y{\rm Pe}^{1/3}$ renders similar contributions to the concentration field from both the diffusion and advection of ions and is asymptotically smaller than the duct thickness d. We expand the concentration distribution in the outer (outside the boundary layer) and inner regions using the series $C = C_0 + {\rm Pe}^{-2/3}C_1 + \cdots$ and $c = c_0 + {\rm Pe}^{-2/3}c_1 + \cdots$, respectively, and further employ Eq. (4) to write the velocity field in the form of an asymptotic series, $\mathbf{u} = \mathbf{u}_0 + \epsilon\mathbf{u}_1 + \cdots$.

Expanding Eq. (1) in the outer region yields the leading order classic result $\mathbf{u}_0\cdot\nabla C_0 = 0$. The leading-order

concentration boundary conditions at the entrance to the duct yield the solution $C_0 = 1$. The leading-order problem in the inner region gives that

$$\begin{aligned} \mathcal{O}(1): \quad & Y\ \partial c_0/\partial x = 2\partial^2 c_0/\partial Y^2, \\ & c_0(Y = h_0) = 0,\ c_0(x = 0) = 1, \\ & c_0(Y \to \infty) = 1, \end{aligned} \tag{5}$$

where we omit the dynamic term, which is proportional to $C_{\text{in}} v_s \ll 1$. In Eq. (5), we expand the velocity field $\mathbf{u}$ about $y \to 0$, retaining the leading-order terms, and using the transformation of the outer coordinate y to the inner coordinate Y. The problem in Eq. (5) is satisfied by a Leveque-type result $c_0 = (3/2)^{1/3}\Gamma(1/3)^{-1}\int_0^\eta e^{-s^3/18} ds$, where $\eta \equiv Y/x^{1/3}$. The leading-order growth rate of the solid metal body is then given by

$$\partial h_0/\partial t = \partial C_0/\partial Y|_{Y=h_0} = (3/2)^{1/3}\Gamma(1/3)^{-1} x^{-1/3}. \tag{6}$$

Assuming that $\epsilon = \mathcal{O}(\text{Pe}^{-1})$ renders a contribution of the dendrites to the concentration field in the leading correction to the ion transport problem along with the leading-order corrections from the ion diffusion and advection mechanisms. Collecting terms that are proportional to Pe^{-1} gives the corresponding equations and boundary conditions. The ion transport in the outer region is governed again by the advection of ions, $\mathbf{u}_0 \cdot \nabla C_1 = 0$, where we omit terms that are proportional to the vanishing derivatives of C_0. The correction to the boundary conditions render the solution $C_1 = 0$. The equation and boundary conditions that govern the transport of ions at the boundary layer (inner region) are given by

$$\begin{aligned} &\mathcal{O}(\text{Pe}^{-2/3}): Y\partial c_1/\partial x + 2u_1\partial c_0/\partial x + 2v_1\partial c_0/\partial Y \\ &\quad = 2\partial^2 c_1/\partial Y^2 + 2\partial^2 c_0/\partial x^2, \\ &\quad c_1(Y = h_0) = -\partial c_0/\partial Y|_{Y=h_0} \times h_1, \\ &\quad c_1(x, Y \to \infty) = C_1(y \to 0) = 0, c_1(x = 0, Y) = 0. \end{aligned} \tag{7}$$

The growth rate of dendrites is then given by

$$\partial h_1/\partial t = \partial C_1/\partial Y|_{Y=h_0}. \tag{8}$$

Both Eqs. (7) and (8) are solved by numerical analysis, which we discuss in the Appendix.

Following our previous insights and as a last note in this part of the paper, it is of value to give a rough estimate of the dimensional length of the boundary layer along the duct. This is to highlight the validity of the two ion transport regimes — the ion concentration boundary layer regime and the developed ion concentration regime to appear past the boundary layer. We define the upper limit of the concentration boundary layer where the concentration field differs by 1% from the outer region concentration: $C_0 = 0.99\, C_{\text{in}}$. By further using the Leveque-type solution to the leading-order boundary layer concentration field in Eq. (5), we obtain that the upper limit of the boundary layer is found at $\zeta \equiv (y/d)\text{Pe}^{1/3}/(x/d)^{1/3} \approx 3.7$, where we use dimensional notation. Further equating $y = d$, where the boundary layer approximately reaches the upper side of the duct, gives that the length of the boundary layer region, relatively to the thickness of the duct, is approximately $x/d = (\text{Pe}^{1/3}(y/d)/\zeta)^3 \approx \text{Pe}/50$. For example, assuming that the characteristic flow velocity is $U = 10$ mm/s, the height of the duct is $d = 1$ mm and the diffusion coefficient of the metal ions is $D = 10^{-3}$ mm^2/s, gives that $\text{Pe} = 10^4$. The approximate length of the concentration boundary layer is $x \approx 200$ mm. Hence, most convective deposition systems support a concentration boundary layer throughout their length. However, it is of value to further consider the physics of dendrite growth past the ion concentration boundary layer.

C. Past the concentration boundary layer (developed region)

Past the concentration boundary layer, we solve an analog of the Graetz problem [50]. The scaling for the vertical coordinate remains the same as before. However, the mass conserving scaling for the horizontal coordinate and vertical velocity in this case are given by d Pe and $U_0\ \text{Pe}^{-1}$, respectively. In addition, our requirement that the timescale is associated with the growth of the metal solid at the bottom of the duct, which translates to keeping both sides of the equality in Eq. (2) of similar magnitude, gives the scaling transformation for time, $t \to (d^2/Dc_{\text{in}}v_s)t$. The dimensionless equation for metal transport in the duct becomes

$$C_{\text{in}} v_s\, \partial C/\partial t + \mathbf{u} \cdot \nabla C = \partial^2 C/\partial y^2 + \text{Pe}^{-2}\, \partial^2 C/\partial x^2, \tag{9}$$

where the velocity field $\mathbf{u}$ is similar to the one in the previous problem and is given in Eq. (4). Moreover, as before, the small parameter $C_{\text{in}} v_s \ll 1$ renders dynamic contributions to our transport problem irrelevant. The corresponding boundary conditions are $C(y = h) = 0$, $C(y = 1) = 1$, $C(x = 0) = R(y)$, where $R(y)$ is a function which represents the concentration distribution of metal in the liquid following the passage of the liquid through the boundary layer region and where we take the obscure entrance to this region to be at $x \to 0$. Moreover, the rate of solid growth is assumed proportional to the diffusive flux of metal to its surface, as in Eq. (2).

We model the growth of the solid surface as previously

$$\begin{aligned} h(x, t) &= h_0(x, t) + \epsilon h_1(x, t) + \cdots \\ &\approx h_0(t) + \epsilon f(t)\sin(kd\text{Pe}\, x) + \cdots, \end{aligned} \tag{10}$$

albeit in the absence of the $\text{Pe}^{-1/3}$ contribution to the leading rate growth of the solid surface, which, as noted before, is a characteristic of ion transport through a boundary layer.

We solve the problem using a regular asymptotic expansions in $\epsilon = \mathcal{O}(\text{Pe}^{-1})$, so that $C = C_0 + \epsilon C_1 + \cdots$, and $\mathbf{u} = \mathbf{u}_0 + \epsilon\mathbf{u}_1 + \cdots$ The leading-order problem is then given by

$$\begin{aligned} \mathcal{O}(1): & u_0\partial C_0/\partial x = \partial^2 C_0/\partial y^2, \\ & C_0(y = h_0) = 0,\ C_0(y = 1) = 1, \\ & C_0(x = 0) = R(y). \end{aligned} \tag{11}$$

We show in the Appendix that the problem in Eq. (11) is satisfied by a series solution that accounts for the initial condition $C_0(x = 0) = R(y)$ at the entrance to this region. However, the series solution fast decays to a linear concentration distribution along the duct

$$C_0(x > 0) = y + \sum_n \beta_n e^{-\lambda_n^2 x} g_{1,n}(\lambda_n) \approx y, \tag{12}$$

which renders the initial distribution of concentration $R(y)$ at $x \to 0$ irrelevant to the transport of ions to the solid surface

at the bottom of the duct in this region, where β_n and $g_{1,n}$ are constants and polynomial eigenfunctions of the eigenvalues λ_n, respectively. Briefly, the eigenvalues are positive and increase in size with their index. For example, the first three eigenvalues are $\lambda_0 = 9.5125$, $\lambda_1 = 20.7736$, and $\lambda_2 = 32.0735$. Hence, the solution of C_0 is a superposition of the linear term y and a fast decaying series of exponents. The first and slowest decaying term in the series of exponents consists of the term $e^{-\lambda_0^2 x} \approx e^{-100x}$. Dimensionally, the later translates to an exponentially decaying function with a decaying length of 1/100 of the characteristic length of the duct, $d\mathrm{Pe}$. Other terms in the series for $g(y)$ decay faster. Hence, the initial condition for the concentration field past the boundary layer $C_0(x = 0) = R(y)$ converges incredibly fast to a linear concentration field, which is a function of the boundary condition at the upper and lower sides of the duct and is independent of $R(y)$. Further details are given in the solution of the leading-order problem in the developed region in the Appendix. Following the above analysis, the corresponding rate of growth of the solid metal body at the bottom of the duct is largely independent of the concentration field near the entrance to the developed region $R(y)$ and is given by

$$\partial h_0/\partial t = \partial C_0/\partial y|_{y=h_0} \approx 1. \tag{13}$$

The leading correction to the above problem, which accounts for the growth of dendrites and requires a numerical solution, detailed in the Appendix, is given by

$$\begin{aligned} \mathcal{O}(\epsilon) : & u_0 \partial C_1/\partial x + u_1 \partial C_0/\partial x + v_1 \partial C_0/\partial y \\ & = \partial^2 C_1/\partial y^2, \\ & C_1(y = h_0) = -\partial C_0/\partial y \times h_1(x), \\ & C_1(y = 1) = 0, \quad C_1(x = 0) = 0, \end{aligned} \tag{14}$$

and

$$\begin{aligned} \partial h_1/\partial t = & -\partial C_0/\partial x \times h_1' + \partial C_1/\partial y|_{y=h_0} \\ & + \partial^2 C_0/\partial y^2|_{y=h_0} \times h_1, \end{aligned} \tag{15}$$

where contributions from the first and third expressions on the right-hand side of the equation vanish since $C_0 \approx y$.

III. RESULTS

A. Ion concentration fields and fluxes

The concentration boundary layer is characterized by intense concentration gradients. The leading order and secondary fluxes of metal ions — the secondary fluxes are the correction to the ion flux in the presence of dendrite hotspots — are proportional to the third root of the Peclet number $\mathrm{Pe}^{1/3}$. We plot in Fig. 2(a) the contribution of the dendrite hotspots, of the order of magnitude $\mathcal{O}(\epsilon)$, to the ion concentration field at the boundary layer C_1 for a dendrite surface density of $kd = 40$. We further magnify the concentration field away from the upstream entrance to the duct in Fig. 2(b). The arc-like contours that can be seen in the later figure emerge from the harmonic deformation of the metal surface (dendrite hotspots). We observe lower and greater levels of concentration above protrusions and depressions, respectively, in the metal surface, which are associated with the transport of metal ions to the dendrite hotspots.

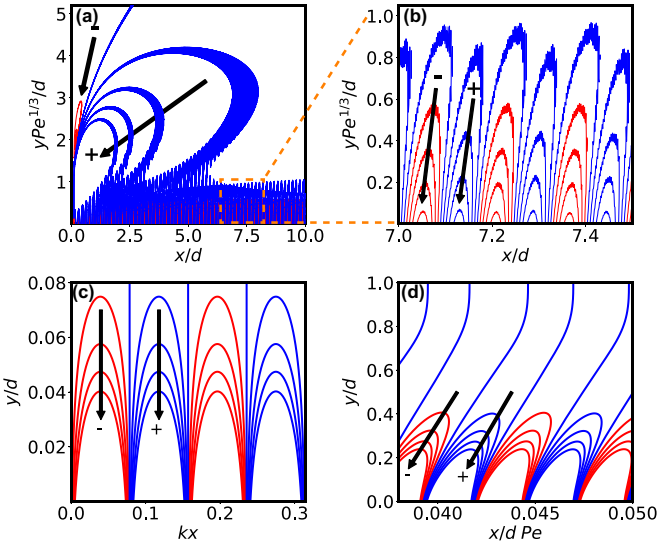

FIG. 2. Concentration correction, C_1, contour plots (relatively to the leading-order concentration fields C_0), where the surface concentration of hotspots for dendrite growth is $kd = 40$ in (a) the boundary layer where we further give (b) a magnification of the contours near the bottom side of the duct, in (c) the absence of flow in the duct, and (d) past the boundary layer where we further assumed $\mathrm{Pe} = 30$. The "+" and "−" signs and arrows indicate the direction of increasing absolute values, respectively, of the contours, which obtain the scaled values of (red) $C_1 = -0.2, -0.15, -0.1, -0.05$, and (blue) $C_1 = 0$, 0.05, 0.1, 0.15, 0.2.

It is of value to compare these results to the diffusive concentration field. The dimensionless number $C_{\mathrm{in}} v_s \ll 1$ renders the problem steady to leading order as before. Keeping the parameters the same as in the ion convection problem and using the same scaling transformations which give Eq. (1), one obtains that the trivial dimensionless ion diffusion problem is governed by the equation and boundary conditions, $\nabla^2 c = 0$, $c(y = h(x)) = 0$, $c(y = 1) = 1$. The diffusion problem is satisfied by the solution $C = y + \epsilon[\coth(kd)\sinh(kd\ y) - \cosh(kd\ y)]\sin(x) + \mathcal{O}(\epsilon^2)$. The first and second terms on the right-hand side of the equation are the concentration field in the absence of dendrite hotspots and the correction to the concentration field due to the presence of the hotspots, respectively. The flux of metal ions to the bottom metal surface is given by Eq. (2).

In Fig. 2(c), we give the order $\mathcal{O}(\epsilon)$ correction to the concentration field due to the presence of dendrite hotspots. In the absence of flow, the concentration contours are symmetrical about the protrusions (hotspots) and depressions at the metal surface. In this case we do not observe "tilted" concentration contours. In the presence of convective flow, the "tilted" isoconcentration contours in Figs. 2(a), 2(b) (boundary layer) and 2(d) (past the boundary layer), indicate convective dispersion in the ion field and hence mixing of ions between low and high concentration regions. The "stretch" or "tilt" in the concentration field is due to ion convection by the Poiseuille-type flow along the duct in Eq. (4).

We further indicate the tendency of the concentration fields in the different ion convective cases to support dendrite growth by plotting the flux of ions to the metal surface

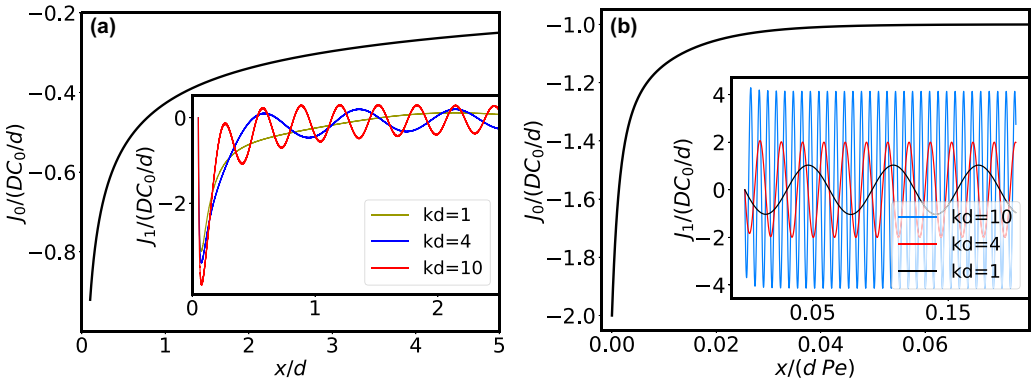

FIG. 3. Spatial (x) variations of ion flux at the bottom side of the duct in the (a) boundary layer and (b) past the boundary layer, where the leading-order solutions for the flux are given in the outset and the second-order solutions, where we account for the presence of hotspots for dendrites, are given in the inset. In the outset of (b) we demonstrate the rapid exponential decay of the leading order flux, which following the concentration field in Eq. (12), is given by $J_0(x>0) = -1 - \sum_n \beta_n e^{-\lambda_n^2 x} d[g_{1,n}(\lambda_n)]/dy$, where in the plot we use the first three terms in the plot and assume $\beta_n = 1/3$. In the inset we demonstrate that an increase in the surface density of hotspots for dendrite growth, kd, renders an increase in the harmonic amplitude of the second-order flux, given here for $\mathrm{Pe} = 100$.

in Fig. 3. We show the leading- and second-order fluxes of ions at the boundary layer in Fig. 3(a) and the inset, respectively. The inset is given for different density concentration of hotspots kd. The dimensional leading-order and second-order fluxes $j_0 \approx -D\partial C_0/\partial Y|_{Y=0}$ and $j_1 \approx -D\partial C_1/\partial Y|_{Y=0}$ (note the stretched Y coordinate), where we omitted vanishing terms, decay along the duct. This is a correction to the ion flux due to the presence of dendrite hotspots.

In the same figure, we further plot the ion fluxes to the metal surface past the boundary layer. This time, the ion fluxes are defined as $j_0 \approx -D\partial C_0/\partial y|_{y=0}$ and $j_1 \approx -D\partial C_1/\partial y|_{y=0}$ (note the unstretched y coordinate), and are given for $\mathrm{Pe} = 100$ and a hotspot surface density of $kd = 40$. We demonstrate the fast spatial decay of the leading-order flux J_0 to a constant value, using the first three terms in the eigenfunction series in Eq. (12). The eigenfunctions transfer information about the concentration of ions at the boundary layer. Their fast decay demonstrates the independence of the ion flux past the boundary layer from its counterpart at the boundary layer, discussed earlier. In the inset we demonstrate the correction to the ion flux C_1, which indicates spatial harmonic variations of the ion concentration along the duct. The harmonic variations of ion flux match the harmonic distribution of hotspots at the metal surface in Eq. (14).

B. Rate of surface growth

In Fig. 4 we isolate the scaled rate of dendrite growth $\dot{h}_1$, [omitting the gauge function ϵ in the second term in the asymptotic series in Eqs. (3) and (10)] as a function of the dendrite density kd. The scaled rate of dendrite growth $\dot{h}_1$ is independent of Pe at the concentration boundary layer and moderately increases with kd in a manner proportional to $kd^{1/3}$. Past the boundary layer, we observe that the scaled quantity $\dot{h}_1$ increases in magnitude with Pe and with kd. It is proportional to $\mathrm{Pe}^{1/3}$ and $kd^{1/3}$. Further details are given in the Appendix.

Hence, in the limit where the rate of dendrite growth is predominantly governed by ion transport, the solid metal surface is inherently unstable. Stabilizing near-equilibrium contributions from surface phenomena, such as surface energy and curvature, are small. Dendrites grow unopposed. However, while the goal of fully eliminating dendrites renders strict requirements, which are usually evaluated by methods of linear stability and are unattainable when employing the ion transport limit for the growth of metal surface in our model, we relax the requirements for dendrite mitigation by employing the concept of *kinetic stability*.

We employ the concept of kinetic stability to compare between the rate of growth of dendrites ϵh_1 and of the bulk solid metal (the baseline for dendrites growth) h_0 in the presence and absence of ion convection. Kinetic stability is a measure which is widely used in the field of colloidal science [51] for analyzing the rate of change in systems whose base states are thermodynamically unstable. Should the change be sufficiently slow at the timescale of interest, the corresponding system may be designated kinetically stable. A reminiscent study [52] employed similar ideas for performing advection diffusion limited aggregation simulations of a growing dendrite under the influence of advection in a potential flow.

We define the dendrite growth measure

$$S_1 = \left| \frac{\epsilon \dot{h}_1/\|\epsilon h_1\|}{\dot{h}_0/\|h_0\|} \right|, \tag{16}$$

where $\dot{h}_0 \equiv \partial h_0/\partial t$, $\dot{h}_1 \equiv \partial h_1/\partial t$, and $\|\epsilon h_1\|$ and $\|h_0\|$ are the orders of magnitude of the dendrite and overall metal electrode thicknesses ϵh_1 and h_0, respectively. The condition S_1 is reminiscent to a measure employed in a previous analysis [53]. To leading order $\|\epsilon h_1\| = \epsilon$ and $\|h\| \approx \|\mathrm{Pe}^{-1/3} h_0\| = \mathrm{Pe}^{-1/3}$, respectively, at the boundary layer region, and $\|\epsilon h_1\| = \epsilon$ and $\|h\| \approx \|h_0\| = 1$, respectively, past the boundary layer. In particular, smaller values of S_1 indicate smaller-scaled rates of growth of dendrites relatively to the scaled rate of growth of the bulk solid metal. Thus, smaller values of S_1 indicate greater kinetic stability of an ion deposition system to dendrite growth.

When estimating S_1 at the boundary layer, we ignore the leading edge of the duct at $x < kd$ (first hotspot along the duct) to avoid the vicinity of the theoretical singular ion flux

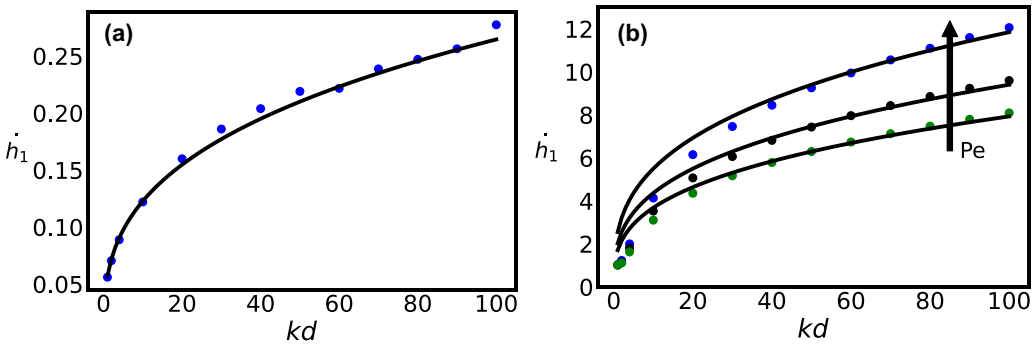

FIG. 4. Scaled rate of dendrite growth (divided by the scaled characteristic dendrite thickness, ϵ) versus the scaled surface concentration of hotspots for dendrite growth (kd) in the presence of (a) the boundary layer and (b) past the boundary layer, where at the boundary layer the result is independent of Pe and approximately proportional to $kd^{1/3}$, and past the boundary layer the result is proportional to $kd^{1/3}$ and $\mathrm{Pe}^{1/3}$ and is given for $\mathrm{Pe} = 1$, 100, and 200. Dots are the product of numerical analysis, and the solid lines are the product of approximate analytical analysis in the Technical Details.

near $x = 0$, where the leading order analytical Leveque-type solution for the concentration boundary layer fails. One may further compare the rate of growth ratio in the presence of convection $S_1(\text{convection})$ and in the absence of convection $S_1(\text{diffusion})$ using the ratio

$$S_2 = \frac{S_1(\text{convection})}{S_1(\text{diffusion})}. \tag{17}$$

In the presence of convective flow in the solution, both S_1 (in the case of convective flow) and S_2 appear in our analysis to mildly vary along the duct at the boundary layer. That is, S_1 varies along the duct in our computational domain by approximately 7%. Outside the boundary layer, S_1 varies along the duct by approximately 0.01%. In the absence of convective flow, S_1 does not change along the duct. Hence, in Fig. 5, we represent S_1 and S_2 as scalars (not as functions of their position along the duct), and consider its variation with the scaled hotspot surface density kd and the Peclet number, Pe.

The ratio between the scaled rates of growth of dendrites and the bulk solid metal (base line), S_1, is independent of the Peclet number Pe at the boundary layer. We plot S_1 in Fig. 5 (a) against the scaled surface density of hotpots for dendrites kd. A first insight to appear in the figure is that $S_1(\text{convection})$ is characteristically smaller than $S_1(\text{diffusion})$ in predominantly convective flow regimes $\mathrm{Pe} \gg 1$. This is emphasized by S_2, which gives the ratio between the two and is characteristically smaller than unity. For example, an ion convective flow in the duct will result in smaller dendrites compared to the case where the ions' transport is solely by diffusion for a specific growth of the bulk solid metal.

In Fig. 5(b), we plot S_1 and S_2 past the boundary layer versus the surface density of dendrite hotspots kd and for different values of the Peclet number, Pe. We find that, in a similar manner to the analysis in the concentration boundary layer, a diffusive transport of ions supports greater rates of growth of dendrites relatively to the rate of growth of the bulk solid metal when this is compared to convective ion transport. Namely, $S_1(\text{convection}) < S_1(\text{diffusion})$ for the same level of kd, as in the case of the boundary layer. Their ratio S_2 is characteristically smaller than unity. Moreover, increasing Pe increases the magnitude of $S_1(\text{convection})$ and S_2. In fact, $S_1(\text{convection})$ and S_2 are linearly proportional to $\mathrm{Pe}^{1/3}$.

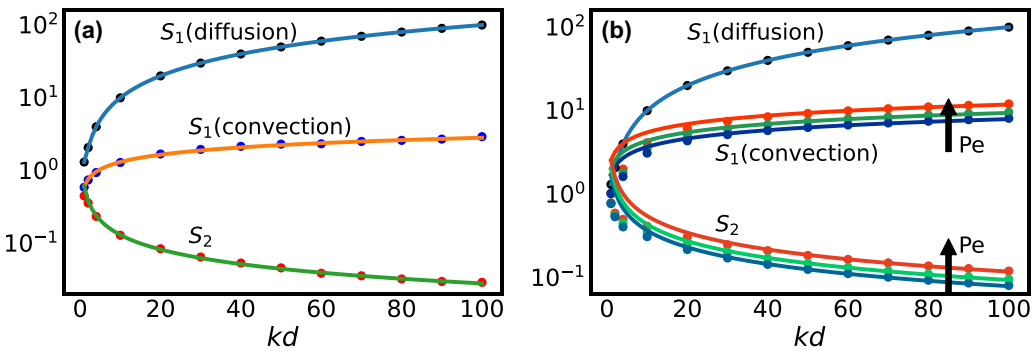

FIG. 5. The measure S_1 for the ratio between the scaled dendrite growth rate and scaled bulk solid metal growth rate in the presence [$S_1(\text{convection})$] and absence [$S_1(\text{diffusion})$] of a ion convection and the measure $S_2 \equiv S_1(\text{convection})/S_1(\text{diffusion})$ versus the scaled surface concentration of hotspots for dendrite growth (kd) at (a) the boundary layer and (b) past the boundary layer, where at the boundary layer, $S_1(\text{convection})$ is independent of Pe and approximately proportional to $kd^{1/3}$, and past the boundary layer, $S_1(\text{convection})$ is proportional to $kd^{1/3}$, and $\mathrm{Pe}^{1/3}$ and is given for $\mathrm{Pe} = 1$, 100, and 200 alongside S_2. Dots are the product of numerical analysis, and the solid lines are the product of approximate analytical analysis in the Technical Details.

IV. DISCUSSION

Electrodeposition and solidification out of a solution of metal ions support the growth of a bulk solid metal, which is usually accompanied by unwanted dendrite growth on the metal surface. To realize the problem of dendrites one must consider both the growth of metal and the growth of dendrites.

The results obtained for the rate of growth of dendrites $\dot{h}_1$ and their relative growth rate compared to the bulk solid metal in the presence and absence of diffusion S_1 and S_2 may now shed light on the controversy about the contribution of convective flow to dendrite growth in the literature. For this analysis one must consider the dimensional rates of growth of dendrites and in particular their timescales $t \sim (d^2/DC_{\rm in}v_s)\mathrm{Pe}^{-2/3}$ and $t \sim (d^2/Dc_{\rm in}v_s)$ at the boundary layer and past the boundary layer, respectively. The dimensional rates of growth of dendrites at and past the boundary layer are given by $(lDC_{\rm in}v_s/d^2)\epsilon\mathrm{Pe}^{2/3}\dot{h}_1$ and $(lDC_{\rm in}v_s/d^2)\epsilon\dot{h}_1$, respectively, where $\dot{h}_1$ is dimensionless as in Fig. 4. Hence, while we expect an unopposed rate of growth of dendrites from the scaled data, we further expect an increase in the rate of growth of dendrites when increasing Pe, when considering its dimensional representation.

In detail, at the concentration boundary layer, the scaled magnitude of the rate of dendrite growth at short times $\dot{h}_1$ is independent of Pe. However, its dimensional representation, $(lDC_{\rm in}v_s/d^2)\epsilon\mathrm{Pe}^{2/3}\dot{h}_1$ is proportional to $\mathrm{Pe}^{2/3}$, assuming for this discussion that we may treat the initial scaled size of the hotspots for dendrite growth $\epsilon \equiv l/d$ constant. Moreover, at the developed region, following the concentration boundary layer, we observe that while the dimensional representation $(lDC_{\rm in}v_s/d^2)\epsilon\dot{h}_1$ lacks an explicit connection to Pe, the scaled quantity $\dot{h}_1$ is proportional to $\mathrm{Pe}^{1/3}$. Our insights are compatible with our mathematical analysis as long as ϵ is of the same order of magnitude as Pe^{-1}, i.e., $\epsilon = \mathcal{O}(\mathrm{Pe}^{-1})$.

While it appears that the presence of convective flow in the solution of ions will increase the rate of growth of dendrites, a judicious assessment of the contribution of convective flow to the ion deposition system should further account for the contribution of ion deposition to the growth of the bulk solid metal. The dimensional rate of growth of the latter at the boundary layer [given in dimensionless terms in Eq. (15)] is proportional to $\mathrm{Pe}^{2/3}$. Their ratio, which we quantify using the measure S_1(convection) in Eq. (16) and demonstrate in Fig. 5, is independent of Pe and may be smaller than S_1(diffusion) (in the absence of convective flow) by orders of magnitude. Hence, while convective flow in the solution enhances the rate of growth of dendrites, it also enhances the rate of growth of the bulk solid metal. Our results indicate that for a fixed rate of growth in the bulk solid metal, one should expect smaller dendrites rate of growth in the presence of convective flow when compared to the case where ions translate though the solution solely by diffusion. Similar insights appear when considering the case of the developed concentration region, past the boundary layer, albeit in the latter case, the measure S_1(convection) is proportional to $\mathrm{Pe}^{1/3}$.

V. CONCLUSION

We solve a problem of dendrite growth at a surface of a duct that undergoes a convective Poiseuille-type flow in a dilute solution of ions. This is a model system, which we employ to resolve the distinct contradiction between different studies as to the contribution of convective flow in a solution to the rate of dendrite growth in the cases of solidification from a solution and electrodeposition.

We assume an ideal model system to predominantly concentrate on the direct contributions of ion convection to the rate of dendrite growth to avoid masking convective effects by the many additional mechanisms that take place in industry-level electrodeposition and solidification systems. In particular, we assume a dilute and isothermal solution of ions, small geometrical protrusions that serve as hotspots for dendrite growth, and avoid dendrite stabilizing mechanisms at the solid surface and within the solid metal by considering the regime where the transport of ions is the rate-determining mechanism for the growth of the solid metal. The last assumption is compatible with far from equilibrium conditions at the metal surface and is akin to the limiting current condition in the case of electrodeposition. An implication of our ion transport limited surface growth assumption is that system-specific dendrite stabilizing mechanisms [11,19,54,55] to appear at near-equilibrium conditions do not contribute to dendrite mitigation in our case.

Our key finding is that ion convection is unequivocally preferable for the mitigation of dendrite growth when compared to the transport of ions by pure diffusion, at least in the ion transport-limited (far from equilibrium) limit considered in this study. We assert the intuitive expectation that the convection of ions in the solution should enhance the growth of dendrites [33,37–42,44]. However, we demonstrate that to further realize the contribution of ion convection to the magnitude of dendrites to appear following metal deposition, one should further compare the rate of growth of dendrites to the rate of growth of the bulk solid metal. We consider the growth rate ratio between the dendrites and the bulk solid metal by employing a measure devised in a previous study [53] S_1. It quantifies the ratio between the relative rate of growth of dendrites h_1 and the relative rate of growth of the bulk solid metal, i.e., the baseline of the metal surface, h_0.

We demonstrate that the relative rate of growth of dendrites always exceeds that of the bulk solid metal in the presence and absence of convective ion transport, i.e., $S_1 > 1$, at least in the far from equilibrium limit. However, we find that the measure S_1 further indicates that the rate of growth of dendrites relatively to the rate of growth of the bulk solid metal is greater in the absence of convective flow, i.e., $S_2 \equiv S_1(\text{convection})/S_1(\text{diffusion}) < 1$. Hence, one may expect the growth of smaller dendrites for a fixed growth of the bulk solid metal in the presence of convective flow compared to the case of ion transport by diffusion. Moreover, increasing the rate of flow, i.e., Pe, will increase the rate of dendrite growth. However, it will not alter the ratio between the rate of growth of dendrites and the bulk solid metal S_1 in the boundary layer regime, and will weakly alter that ratio in a manner proportional to $\mathrm{Pe}^{1/3}$ in the developed region, past the boundary layer.

The benefit in mitigating dendrites by employing the convective transport of ions appears to increase when increasing the surface density of hotspots for dendrite growth. This may be connected to our observation that convective flow in the ion

solution appears to disperse ion concentration in the vicinity of arrays of dendrites. Hence, the convection of ions in the solution appears to mix ion concentration near protrusions and valleys at the solid surface. Hence, ion convection may reduce gradients in ion concentration near the solid surface. Thus, ion convection reduces the enhanced rate by which ions transport to protrusions in the solid substrate, which otherwise supports the autocatalytic mechanisms of dendrite growth. Our conclusions should hold when further accounting for the presence of dendrite stabilizing mechanisms, which explains previous findings about the mitigation of dendrite growth by convective flow [3,18,25,30–32,43].

ACKNOWLEDGMENTS

We are grateful for the Israel Ministry of Energy funding of this project, Grant No. 219-11-129. O.D. is funded by The Miriam and Aaron Gutwirt Memorial fellowship.

APPENDIX: TECHNICAL DETAILS

1. Numerics

We solve Eqs. (7) and (14) using the implicit Euler method for partial differential equations. The maximal numerical relative error in our calculations for the flux of ions is 8%. This specific relative numerical error is obtained in the case of $kd = 1$ in the concentration boundary layer. Other computed cases are associated with smaller levels of relative numerical error. Moreover, it is noteworthy that one will encounter a critical technical difficulty when solving Eq. (7) near the origin of the duct. The concentration in the liquid differs from the concentration at the solid surface, which renders the derivatives of the given analytical solution of the leading-order concentration c_0 singular at that point. Thus, one must alleviate the singularity of the derivatives of the leading-order problem before they are able to solve the second-order problem. The origin of the singularity is the invalidation of the boundary layer assumptions near the leading upstream edge of the duct. Briefly the boundary layer assumption in the above analysis requires that the concentration distribution transverse to the duct surface changes much faster than along the surface. Thus, the characteristic lengthscales transverse and along the boundary layers are given by $d\mathrm{Pe}^{-1/3}$ and d, respectively; the first is asymptotically smaller than the second. However, sufficiently near the leading upstream edge of the duct, one encounters a region where $x = \mathcal{O}(d\mathrm{Pe}^{-1/3})$ away from the origin (upstream edge of the duct). Hence, due to a geometrical constraint, the lengthscale along the bottom surface of the duct is similar to the one which is transverse to the boundary layer.

To alleviate the flux singularity at the upstream edge of the duct, at $x = 0$, we commence our analysis using the transport equation $C_{yy} + C_{xx} = \mathrm{Pe}\, y\, C_x$ in Eq. (1), where we omitted the dynamic terms using the usual assumption that $C_{\mathrm{in}} v_s \ll 1$. We Strain both coordinates using the transformations $x \to X/\mathrm{Pe}^{1/3}$, $y \to Y/\mathrm{Pe}^{1/3}$. The transport equation transforms to $\mathrm{Pe}^{-1/3}(\mathcal{C}_{YY} + \mathcal{C}_{XX}) = Y\, \mathcal{C}_X$. Expanding the concentration in the asymptotic series $\mathcal{C} = \mathcal{C}_0 + \mathrm{Pe}^{-1/3}\, \mathcal{C}_1 + \ldots$, the leading order $\mathcal{O}(1)$ component of the governing equation is $Y\, \mathcal{C}_{0X} = 0$. Hence, the concentration field C_0 is in the outer region at a characteristic separation of $d\mathrm{Pe}^{-1/3}$ away from the solid. The requirements for the concentration field entering the duct, $C_0(X = 0, Y) = 1$, is satisfied by the solution for the concentration field, $C_0(X, Y) = 1$. The requirement for a vanishing concentration field at the lower surface of the duct, $c_0(X, Y = 0) = 0$, is to be satisfied by a boundary layer of the transverse lengthscale $d\mathrm{Pe}^{-1/2}$; the transverse lengthscale is asymptotically smaller than the characteristic length of the boundary layer downstream, discussed above, $d\mathrm{Pe}^{-1/3}$. Using a procedure equivalent to matched asymptotic expansion along the surface of the duct, one may use the insight that $\partial c_0/\partial x|_{x\to 0} = \partial C_0/\partial X|_{X\to\infty} = 0$ and $\partial c_0/\partial Y|_{x\to 0} = \partial C_0/\partial Y|_{X\to\infty} = 0$ in Eq. (7) to alleviate the singularity of these derivatives at $x = 0$.

2. Solution of the leading-order problem in the developed region

We solve the leading-order problem of the concentration field past the boundary layer in Eq. (11) by a superposition of two simpler problems, which are given by

$$\begin{aligned} &u_0 C_{A,0x} = C_{A,0yy}, \\ &C_{A,0}(x, y = 0) = 0, \quad C_{A,0}(x, y = 1) = 1, \\ &C_{A,0}(x = 0, y) = y \end{aligned} \tag{A1}$$

and

$$\begin{aligned} &u_0 C_{B,0x} = C_{B,0yy}, \\ &C_{B,0}(x, y = 0) = 0,\ C_{B,0}(x, y = 1) = 0, \\ &C_{B,0}(x = 0, y) = R(y) - y. \end{aligned} \tag{A2}$$

The problem in Eq. (A1) is satisfied by the solution $C_{A,0}(y) = y$. We will show next that the solution of the superimposed problem vanish near $x = 0$ and hence may be ignored to leading order. We solve the problem in Eq. (A2) by the separation of variables [50] $C_{B,0} = p(x)g(y)$, which gives the two problems

$$\begin{aligned} &p' + \lambda_n^2 p = 0, \text{ and } g'' + u_0 \lambda_n^2 p = 0, \\ &g(y = 0) = g(y = 1) = 0, \end{aligned} \tag{A3}$$

where the initial condition $p(x = 0)$ is given as part of the solution and λ_n is an eigenvalue of index n of the problem on the right-hand side of Eq. (A3). The general solution of the problem on the left-hand side of Eq. (A3) is given by $p = P_n\, e^{-\lambda_n^2 x}$, where P_n is a constant of integration in x. We represent the two linearly independent solutions of the second-order ODE on the right-hand side of Eq. (A3) using the power series $g_{1,n}(y; \lambda_n) = \sum_{i=0}^{\infty} \alpha_{1,i}(\lambda_n) y^i$ and $g_{2,n}(y; \lambda_n) = \sum_{i=0}^{\infty} \alpha_{2,i}(\lambda_n) y^i$, where $\alpha_{1,i}$ and $\alpha_{2,i}$ are functions of λ_n. Substituting the two solutions in the problem, gives the recursion relation $\alpha_{j,i} = -(\lambda_n^2/2)[(\alpha_{j,i-3} - \alpha_{j,i-4})/i(i-1)]$, wherein $i = 4, 5, 6, \ldots$, and $\alpha_{j,0}$ and $\alpha_{j,1}$ are free parameters, which may be determined from the boundary conditions. The general solution of the problem is $g(y) = \alpha_{1,1} g_{1,n} + \alpha_{2,0} g_2$, where $g_{1,n} = y + (\lambda_n^2/12)y^4 + \ldots$ and $g_{2,n} = 1 + (\lambda_n^2/6)y^3 + \ldots$. We discard the function $g_{2,n}$ since it does not satisfy the boundary conditions at $y = 0$ in Eq (A3). Using the additional condition, we obtain that $g(y = 1) = \alpha_{1,1} g_{1,n} = 0$; the requirement $g_{1,n} = 0$ translates to a polynomial equation in λ_n. We solve the polynomial by using an iterative procedure, where one must employ a large number of significant figures to maintain solution precision and where

we employ the connections $g_{1,n}|_{y=1} = 1 + \alpha_{1,4} + \alpha_{1,5} \ldots$ and $\partial g_1/\partial\lambda|_{y=1} = \partial\alpha_{1,4}/\partial\lambda + \partial\alpha_{1,5}/\partial\lambda + \ldots$ in the framework of the Newton-Raphson iterative approach $\lambda_{n,k+1} = \lambda_{n,k} - g_1|_{y=1}/\partial g_1/\partial\lambda|_{y=1}$. In the second of these, k is the index of iterations. The eigenvalues, which we obtain using this procedure, increase in magnitude with their index. For example, the first three eigenvalues are $\lambda_0 = 9.5125$, $\lambda_1 = 20.7736$, and $\lambda_2 = 32.0735$. Ones we have obtained the eigenvalues λ_n we are able to calculate the constants $\alpha_{1,i}$ and define the eigenfunctions $g_{1,n}(y;\lambda_n)$. The solution of the problem in Eq. (11) is given by the series $C_0 = y + \sum_{n=0}^{\infty} \beta_n e^{-\lambda_n^2 x} g_{1,n}(y;\lambda_n)$, where β_n are constants that help satisfy the initial condition $C_0(x = 0, y) = R(y)$ in Eq. (11). The solution of C_0 is a superposition of the term y and a fast decaying series of exponents. The first and slowest decaying term in the series of exponents consists of the term $e^{-\lambda_0^2 x} \approx e^{-100x}$. In dimensional terms, the last term translates to an exponentially decaying function with a decaying length of $1/100$ of the characteristic length of the duct $d\mathrm{Pe}$. Other terms in the series for $g(y)$ decay faster. In conclusion, the initial condition for the concentration field past the boundary layer $C_0(x = 0) = R(y)$ converges incredibly fast to the linear concentration field in Eq. (12)

$$C_0(x > 0) = y + g(y) = y + \sum_n \beta_n e^{-\lambda_n^2 x} g_{1,n}(y;\lambda_n) \approx y.$$

3. Qualitative connection between dendrite growth ratio Pe and *kd*

One may derive a semi-qualitative representation of S_1(Convection) as a function of the surface density of hotspots for dendrite growth kd. In the case of the boundary layer, the characteristic lengthscales which govern the leading-order solution are the thickness of the duct d and the characteristic thickness of the boundary layer $d\mathrm{Pe}^{-1/3}$ along and transverse to the duct surface, respectively. The corresponding transformations $x \to dx$, $y \to d\mathrm{Pe}^{-1/3}Y$ and $u \to U_0 u$ give the dimensionless and steady transport equation $u_0\ \partial c_0/\partial x = \partial^2 c_0/\partial Y^2$. Dendrite contributions to the concentration field appear in the second-order transport problem, which is governed by the wavelength k^{-1} and the characteristic thickness of the boundary layer, $d\mathrm{Pe}^{-1/3}$, along and transverse to the bottom surface, respectively. The corresponding transformations $x \to k^{-1}x$, $y \to d\mathrm{Pe}^{-1/3}Y$ and $u \to U_0 u$ give the homogeneous part of the dimensionless and steady transport equation $u_0\ \partial c_1/\partial x = (kd)^{-1}\partial^2 c_1/\partial Y^2$, where we employed the usual transformation $y \to d(\mathrm{Pe})^{-1/3}\mathcal{Y}$ to render the problem dimensionless and stretch the y coordinate at the boundary layer. Thus, to render advective and diffusive terms of the same magnitude, we consider a different characteristic boundary layer thickness in the second-order analysis and employ the alternative transformation $y \to d(kd\mathrm{Pe})^{-1/3}\mathcal{Y}$. This transformation gives $u_0\ \partial c_1/\partial x = \partial^2 c_1/\partial\mathcal{Y}^2$. Therefore $h_1 = \partial c_1/\partial y \sim (kd\mathrm{Pe})^{1/3}$. Using scaling analysis, Eq. (2), and remembering that $h_0 = \partial c_0/\partial y \sim (\mathrm{Pe})^{1/3}$, it is straightforward to demonstrate that $S_1 = (\epsilon\dot{h}_1/\|\epsilon h_1\|)/(\dot{h}_0/\|h_0\|) = (\partial c_1/\partial y)/(\partial c_0/\partial y) = kd^{1/3}(\partial c_1/\partial\mathcal{Y})/(\partial c_0/\partial Y)$. Hence, to leading order, $S_1 \approx \gamma \times kd^{1/3}$, where γ is a function of the rest of the parameters in the problem. In a similar manner to the above, one may show that past the boundary layer $S_1 \approx \gamma \times (\mathrm{Pe} \times kd)^{1/3}$. These expressions are used to plot the continuous curves for S_1(convection) and S_2 in Fig. 5.

[1] C. Tubandt, Akad. Verlagsgesellschaft, Leipzig **12** (1932).
[2] T. B. Reddy, *Linden's Handbook of Batteries* (McGraw-Hill Education, New York, 2011).
[3] A. Huang, H. Liu, O. Manor, P. Liu, and J. Friend, Adv. Mater. **32**, 1907516 (2020).
[4] Z. Yuan, X. Liu, W. Xu, Y. Duan, H. Zhang, and X. Li, Nat. Commun. **9**, 3731 (2018).
[5] M. D. Pritzker and T. Z. Fahidy, Electrochim. Acta **37**, 103 (1992).
[6] P. Albertus, S. Babinec, S. Litzelman, and A. Newman, Nature Energy **3**, 16 (2018).
[7] M. A. Jaafar, D. R. Rousse, S. Gibout, and J. P. Bedecarrats, Renewable Sutainable Energy Rev. **74**, 1064 (2017).
[8] A. Sharma, V. V. Tyagi, C. R. Chen, and D. Buddhi, Renewable Sustainable Energy Rev. **13**, 318 (2009).
[9] M. M. Farid, A. M. Khudhair, S. A. K. Razack, and S. Al-Hallaj, Energy Convers. Manage.: X **45**, 1597 (2004).
[10] D. Aurbach, E. Zinigrad, Y. Cohen, and H. Teller, Solid sState Ionics **148**, 405 (2002).
[11] M. D. Tikekar, L. A. Archer, and D. L. Koch, Sci. Adv. **2**, e1600320 (2016).
[12] P. Bai, J. Li, F. R. Brushett, and M. Z. Bazant, Energy & Environmental Science **9**, 3221 (2016).
[13] P. Bai, J. Guo, M. Wang, A. Kushima, L. Su, J. Li, F. R. Brushett, and M. Z. Bazant, Joule **2**, 2434 (2018).
[14] J.-I. Yamaki, S.-I. Tobishima, K. Hayashi, K. Saito, Y. Nemoto, and M. Arakawa, J. Power Sources **74**, 219 (1998).
[15] M. Chamoun, B. J. Hertzberg, T. Gupta, D. Davies, S. Bhadra, B. Van Tassell, C. Erdonmez, and D. A. Steingart, NPG Asia Materials **7**, e178 (2015).
[16] Y.-D. Cho and G. T.-K. Fey, J. Power Sources **184**, 610 (2008).
[17] C. Monroe and J. Newman, J. Electrochem. Soc. **151**, A880 (2004).
[18] J. Jorne, Y. J. Lii, and K. E. Yee, J. Electrochem. Soc. **134**, 1399 (1987).
[19] R. Aogaki, K. Kitazawa, Y. Kose, and K. Fueki, Electrochim. Acta **25**, 965 (1980).
[20] C. Monroe and J. Newman, J. Electrochem. Soc. **150**, A1377 (2003).
[21] E. Khoo, H. Zhao, and M. Z. Bazant, J. Electrochem. Soc. **166**, A2280 (2019).
[22] J. M. Huth, H. L. Swinney, W. D. McCormick, A. Kuhn, and F. Argoul, Phys. Rev. E **51**, 3444 (1995).
[23] V. Fleury, J.-N. Chazalviel, and M. Rosso, Phys. Rev. E **48**, 1279 (1993).
[24] R. Sekerka, S. Coriell, and G. McFadden, J. Cryst. Growth **154**, 370 (1995).
[25] H. J. Scheel, J. Cryst. Growth **211**, 1 (2000).
[26] M. Skyllas-Kazacos, M. Chakrabarti, S. Hajimolana, F. Mjalli, and M. Saleem, J. Electrochem. Soc. **158**, R55 (2011).

[27] J. Lee, K. Kim, S. H. Park, G. Y. Yoon, J. Kim, and S. J. Lee, Nano Energy **77**, 105130 (2020).
[28] M. M. Jakšić, J. Electroanal. Chem. Interfacial Electrochem. **249**, 35 (1988).
[29] M. M. Jaksic and V. P. Komnenic, J. Electroanal. Chem. **328**, 127 (1992).
[30] J. Czochralski, Zeitschrift für physikalische Chemie **92U**, 219 (1918).
[31] J. Aleksic, P. Zielke, and J. A. Szymczyk, Ann. NY Acad. Sci **972**, 158 (2002).
[32] A. Kokh, L. Mironova, and V. Popov, Fluid Dyn. **37**, 667 (2002).
[33] S. Tajima and M. Ogata, Electrochim. Acta **15**, 61 (1968).
[34] M. N. Parekh, C. D. Rahn, and L. A. Archer, J. Power Sources **452**, 227760 (2020).
[35] M. N. Parekh and C. D. Rahn, J. Electrochem. Soc. **167**, 160525 (2020).
[36] M. C. Ma, G. Li, X. Chen, L. A. Archer, and J. Wan, Sci. Adv. **7**, eabf6941 (2021).
[37] M. Glicksman and S. Huang, Adv. Space Res. **1**, 25 (1981).
[38] R. Ananth and W. N. Gill, J. Cryst. Growth **108**, 173 (1991).
[39] R. Ananth and W. N. Gill, J. Cryst. Growth **91**, 587 (1988).
[40] P. Bouissou and P. Pelce, Phys. Rev. A **40**, 6673 (1989).
[41] D. V. Alexandrov and P. K. Galenko, Phys. Rev. E **87**, 062403 (2013).
[42] D. V. Alexandrov and P. K. Galenko, Phys. Chem. Chem. Phys. **17**, 19149 (2015).
[43] R. T. Delves, J. Cryst. Growth **3-4**, 562 (1968).
[44] S. R. Coriell, D. T. Hurle, and R. F. Sekerka, J. Cryst. Growth **32**, 1 (1976).
[45] J.-N. Chazalviel, Phys. Rev. A **42**, 7355 (1990).
[46] J. Zheng, J. Yin, D. Zhang, G. Li, D. C. Bock, T. Tang, Q. Zhao, X. Liu, A. Warren, Y. Deng *et al.*, Sci. Adv. **6**, eabb1122 (2020).
[47] L. G. Leal, *Advanced Transport Phenomena: Fluid Mechanics and Convective Transport Processes*, Vol. 7 (Cambridge University Press, Cambridge, England, 2007).
[48] A. Lévêque, Ann. Mines **119**, 201 (1928).
[49] P. R. Unwin and R. G. Compton, J. Electroanal. Chem. Interfacial Electrochem. **274**, 249 (1989).
[50] G. M. Brown, AIChE J. **6**, 179 (1960).
[51] J. Matusiak and E. Grzadka, Annales Universitatis Mariae Curie-Sklodowska, sectio AA–Chemia **72**, 33 (2017).
[52] M. Z. Bazant, J. Choi, and B. Davidovitch, Phys. Rev. Lett. **91**, 045503 (2003).
[53] W. W. Mullins and R. F. Sekerka, J. Appl. Phys. **34**, 323 (1963).
[54] C. Monroe and J. Newman, J. Electrochem. Soc. **152**, A396 (2005).
[55] Z. Ahmad and V. Viswanathan, Phys. Rev. Lett. **119**, 056003 (2017).